Nuclear Engineering and Technology 54 (2022) 1030–1036

Contents lists available at ScienceDirect

Nuclear Engineering and Technology

journal homepage: www.elsevier.com/locate/net

Original article

A prototype of the SiPM readout scintillator neutron detector for the engineering material diffractometer of CSNS

Qian Yu [a, b, c], Bin Tang [b, c, *], Chang Huang [c, d], Yadong Wei [g], Shaojia Chen [b, c], Lin Qiu [c, e], Xiuku Wang [b, c], Hong Xu [b, c], Zhijia Sun [b, c], Guangyou Wei [c, f], Mengjiao Tang [c, h]

[a] University of Chinese Academy of Sciences (UCAS), Beijing, 100049, China
[b] Institute of High Energy Physics, Chinese Academy of Sciences(CAS), Beijing, 100049, China
[c] Spallation Neutron Source Science Center (SNSSC), Dongguam, 523803, China
[d] Lanzhou University, No. 222 South Tianshui Road, Lanzhou, 730000, China
[e] Southwest University of Science and Technology, Mianyang, 621002, China
[f] Xi'an Jiaotong University, Xi'an, 710049, China
[g] Institute of Science Techology Innovation, Dongguan University of Technology, Dongguan, 523800, China
[h] Zhengzhou University, Zhengzhou, 450001, China

ARTICLE INFO

Article history:
Received 8 April 2021
Received in revised form
31 August 2021
Accepted 14 September 2021
Available online 18 September 2021

Keywords:
SiPMs
Wavelength-shifting fibres
Neutron detector,6LiF/ZnS(Ag)
ASIC

ABSTRACT

A high detection efficiency thermal neutron detector based on the ^{6}LiF/ZnS(Ag) scintillation screens, wavelength-shifting fibers (WLSF) and Silicon photomultiplier (SiPM) readout is under development at China Spallation Neutron Source (CSNS) for the Engineering Material Diffractometer (EMD).A prototype with a sensitive volume of 180mm×192mm has been built. Signals from SiPMs are processed by the self-design Application Specific Integrated Circuit (ASIC).

The performances of this detector prototype are as follows: neutron detection efficiency could reach 50.5% at 1 Å, position resolution of 3, the dark count rate <0.1Hz, the maximum count rate >200KHz. Such detector prototype could be an elementary unit for applications in the EMD detector arrays.

1. Introduction

Neutron scattering techniques are playing an important role in the study of material structure and dynamic properties, which are widely used in various subjects [1,2]. Advanced neutron sources are the basis of neutron science research. As the first spallation neutron source in developing countries, the China Spallation Neutron Source (CSNS) project has been running steadily from March 2018. In the first phase of the CSNS, three instruments have been built and are operating routinely [3]. They are open to users all around the world since 2018. According to the construction plan of CSNS, the new instrument EMD (engineering material diffractometer) will be installed in Aug.2022.

EMD is a neutron time-of-flight (TOF) diffractometer which is designed to function as a strain scanner for the investigation of residual stress in engineering materials and components. It needs a neutron detector with a sensitive area of more than $3m^2$ to cover the 90° neutron diffraction angle region. The ^{3}He tube is one of the ideal neutron detectors for many neutron spectrometers. However, owing to the world-wild shortage of ^{3}He and the increasing cost, seeking new neutron detectors to replace the ^{3}He tube is urgent. The advantages of scintillator detector including high position resolution, low n/γ rejection ratio, real-time detection make it widely used in many neutron instruments, including strain scanners [2,4,5].

We have developed scintillator neutron detectors since 2011 [6–8]. A detector with an active area of more than $5m^2$ covering area based on the ZnS(Ag) screens, wavelength-shifting fibers (WLSF) arrays and multi-anode photo multiplier tubes (MA-PMT) had been installed in GPPD (General Purpose Powder Diffractometer) in the middle of 2017. The position resolution of this detector is 4mm×4 mm and the thermal neutron detection efficiency is about 45% at 2 Å. All these detectors are working well in the instrument and have been running since 2018. However, there are some disadvantages, such as poor uniformity of detection

* Corresponding author. Institute of High Energy Physics, China.
E-mail address: tangb@ihep.ac.cn (B. Tang).

https://doi.org/10.1016/j.net.2021.09.014

efficiency, high cost and complicated manufacturing; especially the inhomogeneity of detection efficiency, which is mainly caused by the gain inhomogeneity of the MA-PMT. It directly affects the confidence interval of the sample test results from the instrument.

According to the physical design of the EMD, the detector should fulfill the parameters as shown in Table 1.

In order to solve this problem, we are currently developing a SiPM readout scintillation neutron detector based on oblique ^{6}LiF/ZnS(Ag) scintillator screens, wavelength-shifting fibers and SiPMs readout. As an alternative to the MA-PMT, the SiPMs, which consist of thousands of avalanche photodiodes working in Geiger-mode, have several advantages such as relatively low operation cost, much lower operating voltages, compactness, and their operability in magnetic fields.

SiPMs have similar gains to that of the MA-PMT and higher quantum efficiency. Most importantly, due to the development of semiconductor fabrication technology, the gain uniformity of the SiPMs between each device is decent, which could improve the non-uniformity in the detection efficiency of the detector.

In this work we built a 192mm×180 mm sensitive area detector prototype with SiPM readout and electronics of our own design. The performance of the prototype including detect efficiency, maximum count rate and the position resolution, has been obtained in the CSNS neutron beam line.

2. The detector structure

Fig. 1 shows the schematic diagram of the SiPM readout scintillator detector. The head of the detector consisted of several oblique ^{6}LiF/ZnS(Ag) screens and WLS fibers. The screens are placed at the same specified angle, and are fixed in the positioning slots. Two WLS fibres are uniformly distributed under each screen to collect the scintillating photons. The ends of the fibres polished and coupled to the SiPMs. Aluminum reflective films are attached above and below the scintillator screens to increase the reflection of the scintillation photons.

The oblique angle of the scintillator screens to the incident neutrons is 17°. This design increases the path of incidence neutrons to improve the detection efficiency without increasing the emission path of the scintillating photons. The signals from each SiPM are amplified, shaped, and discriminated by the our own electronics. Then the TOF and the pixel position of the neutron signals are recorded and transmitted by the FPGA module of the electronics. All the position and time information of the detector is uploaded to the terminal PC through an optical fiber.

Table 1
The main parameters of detector modules for EMD.

main technical parameters	parameter index
detection efficiency	> 40%@1 Å
spatial resolution	3mm × 180 mm
maximum count rate	>30KHz/pixel
gamma-ray sensitivity	$<10^{-5}/^{60}Co$
Dark count rate/pixel	*0.*1Hz/*pixel*
pixel to pixel detection efficiency uniformity	*<20%*

3. Key components performance

The key components of this SiPM readout scintillator neutron detector are the ^{6}LiF/ZnS(Ag), the WLSF, the SiPMs and the electronics. Through the research of the detectors for the GPPD, the ^{6}LiF/ZnS(Ag) from AST with mass ratio of 1 : 2 and 400 μm thickness and the WLSF from Kuraray with 1mm diameter (Y-11 (200)MS) are still suitable [9,10]. We need to select the SiPMs and design the special electronics.

3.1. The SiPMs performance and the selection

For the scintillator neutron detector, the SiPM device needs to have high quantum efficiency, high gain, low dark noise, small temperature drift and low working bias [5,11,12]. Considering that one end of each of two 1 mm-diameter WLSFs need to be coupled to the SiPM entrance window, the effective working area of the SiPM device needs to be about 3mm×3mm. Two suitable SiPMs were selected as the candidates, S13363-3050 from Hamamatsu and MicroFC-30035 from Sensl [13,14]. Table 2 shows the main parameters of these two types of SiPM. The characteristics of the SiPMs were measured to select the best SiPM for the detector.

We measured the volt-ampere characteristic curves to verify their avalanche critical voltage [15,16]. Fig. 2 shows the measurement result that the avalanche voltage of the S13363- 3050 is 52.5V, while the avalanche voltage of the MicroFC-30035 is 24.5V. Both are consistent with the manufacturer's specifications.

The gains of the SiPMs are tested with a blue LED light which is triggered by external pulsed signals to control the luminous time

Table 2
Specifications of SiPMs.

	Hamamatsu	Sensl
Type	S13363-3050	MicroFC-30035
Sensitive area	3mm×3mm	3mm×3mm
Breakdown voltage	52.5V	24.5V
Over voltage	2.5V	2.5V
Gain	3.4 × 10^{6}	4 × 10^{6}
PDE/480 nm	32%	24%
temperature coefficient	55 mV/°C	21.3 mV/°C

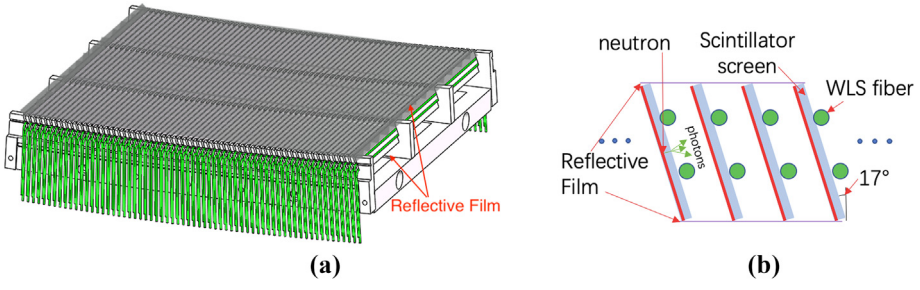

Fig. 1. (a) is the detector unit which is used for performance studies (b) is the detailed structure of the detector.

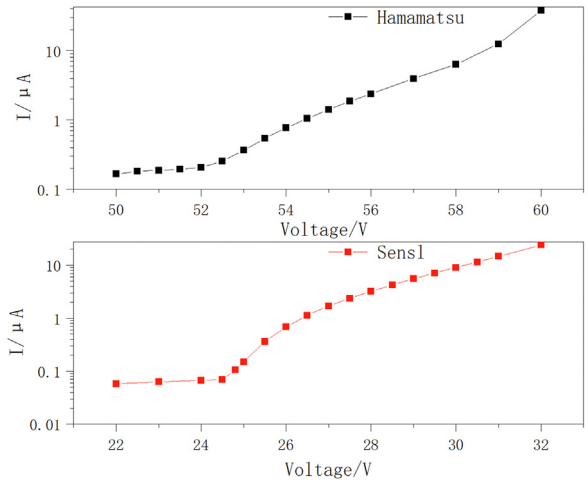

Fig. 2. is the V–I curve of Hamamatsu and Sensl SiPMs, from which we can find out that the breakdown voltage is consistent with the manufacture's specifications.

and luminous intensity. Fig. 3 shows the signals from a SiPM when it was illuminated with the pulsed light from the LED and then amplified with a line amplifier and observed with an oscilloscope. When the trigger voltage of the LED is changed, the numbers of photons detected by the SiPM is also changed. Using an integrating amplifier and a standard DAQ system, the integral charge spectrum for different numbers of photons from the SiPMs is obtained. Fig. 4 shows the integral charge spectrum of the SiPMs. The gain of the SiPMs can be obtained by calculating the difference of each signal peak position in the integral charge spectrum as shown in the formula below:

$$\text{Gain} = \Delta Q \times \text{ADC}/e \quad (1)$$

Where ΔQ is the difference value between two peaks and ADC is the conversion factor between charge value and the channel number of the standard DAQ system. The e is the charge of an electron: 1.6×10^{-19}C.

Fig. 5(a) shows the gain curve of the two SiPMs with different bias voltage. As expected, the greater the bias voltage applied to the SiPM, the greater the gain. The gain of MicroFC-30035 is greater than that of the S13363 which is also consistent with the manufacturer's specifications. By changing the environmental temperature of the SiPMs in an enclosed box, we also determined how the gain varied with different temperature as shown in Fig. 5(b) [17]. The higher the environmental temperature, the smaller the gain of the SiPM. We calculated that the temperature coefficient of the MicroFC-30035 is 21.3mV/°C and that of the S13363 is 55mV/°C. In the subsequent design of the SiPM power supply module, the temperature drift compensation module will be added according to these test results, so MicroFC-30035 is selected as the preferred candidate.

3.2. The readout electronics system

The readout electronics for this scintillator detector were designed by our electronics group. Fig. 6(a) is the electronic board, which consists of ASIC and data acquisition mother board; 6(b) shows the structure diagram. The structure of "sub-board-main-board" is adopted to realize the integration and flexibility of the electronic readout system. The front amplifier uses an application specific integrated circuit (ASIC) to fulfill analog signal processing such as amplification, shaping and discrimination. The mother-board firmware adopts the design method of a multi-level pipeline

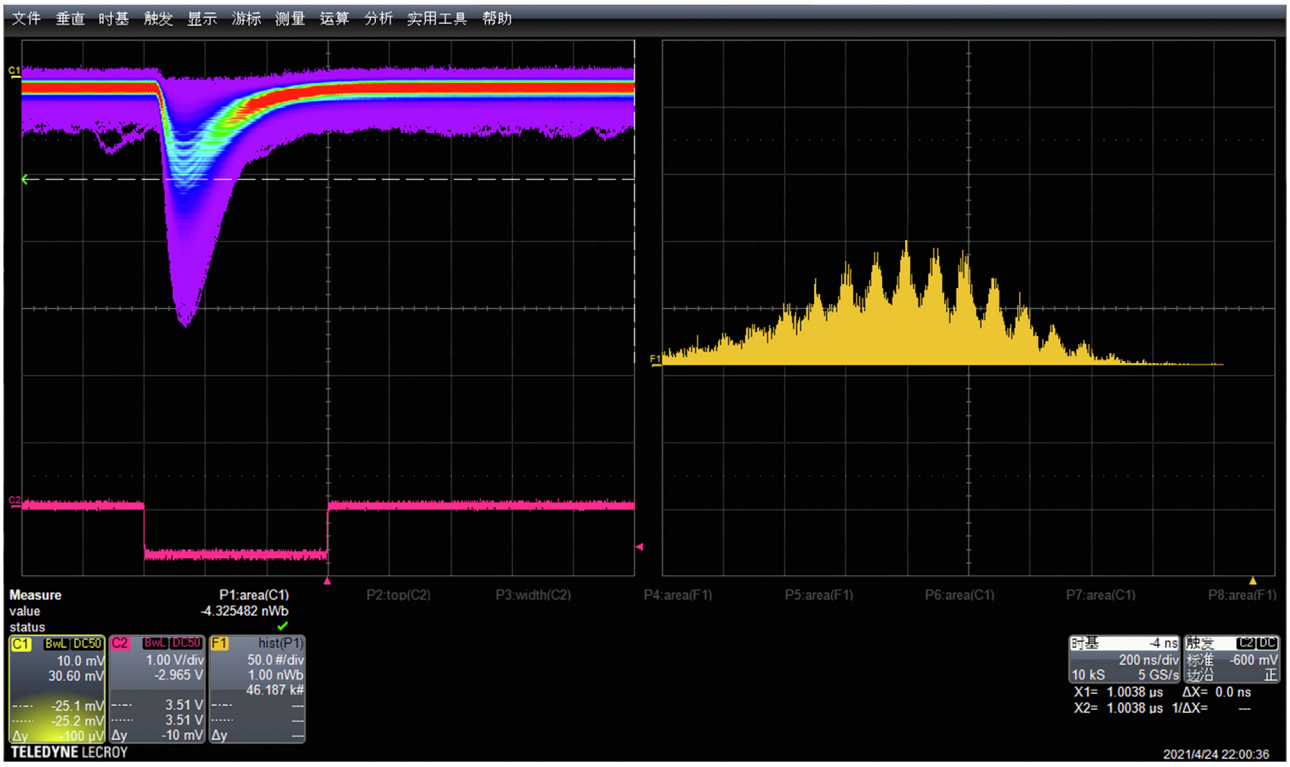

Fig. 3. Shows the signals from a SiPM which is illumined by blue LED light. (For interpretation of the references to colour in this figure legend, the reader is referred to the Web version of this article.)

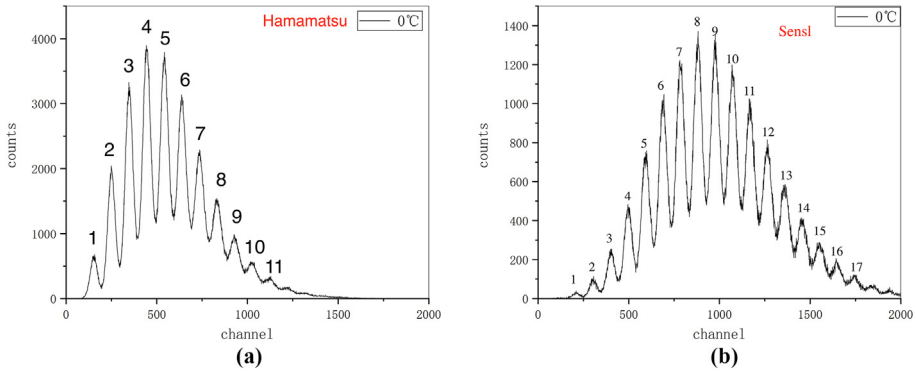

Fig. 4. (a) and (b) shows the integral spectra of signals in the gate from the two different SiPMs.

mechanism to realize the data acquisition, packaging, caching and other processing.

In order to reduce the influence of the high dark count rate from the SiPM, a voltage sensitive preamplifier and a discriminator with an adjustable threshold and pulse width were adopted in the design. The electronics excludes the neutron signals with thresholds and pulse widths smaller than the set value. The final data is transmitted to the back-end data processing system through Gigabit Ethernet for data analysis and processing. The information of the position, the width and the time of each neutron signal is recorded by the readout electronics. The SiPM power supply module, temperature probe and temperature compensation circuit are integrated on the readout electronics board to ensure the gain stability of the SiPMs.

4. The prototype detector

A prototype with a 192mm × 180 mm sensitive area has been equipped with 64 inclined ^{6}LiF/ZnS(Ag) scintillator screens (see Fig. 7). The oblique angle of the scintillator screens to the incident neutrons is 17°. This is the minimum angle for the mechanical design when optimising neutron absorption efficiency, minimum dead area and maximum light collection. 128 1-mm diameter WSL fibers are uniformly distributed over the scintillator screens.This structure defines the 3mm×180mm pixel size and 64 pixel channels. The 32 FC30035 SiPMs are seamlessly packed into a line on a single PCB board. There are two SiPMs lines for the 64 pixel channels of the detector prototype. The WLS fibers are bent in a 3mm radius using a special hot water bending method to reduce the dead area of the detector. The ends of each fibre are polished and coupled to the SiPMs by support bases. The entire prototype assembly is about 200 mm × 200 mm × 340 mm and is light tight after assembly.

We tested the detection efficiency of the prototype on the neutron beam line #20 of CSNS. BL20 uses a decoupled narrow liquid hydrogen moderator. Neutrons are collimated by the chopper and neutron guide, the diameter of the neutron beam spot at the outlet is 45 mm, the neutron flux rate is about 10^{6}n/(cm^{2}s) and the neutron wavelength range is 0–10 Å. The distance from moderator to the neutron outlet spot is about 9m.

Fig. 8 shows the instrument layout of the detection efficiency measurement. Because the distribution of the neutron wavelength from BL20 is wide, a germanium [220] monochromator was used to reduce the neutron intensity and select the special neutron wavelength. A standard ^{3}He tube with 20atm pressure and 1-inch diameter (252315,LND) was used to measure the incident neutron intensity from a shielding slit with a width of 1mm. Then the standard ^{3}He tube was moved away, and the neutron intensity was measured with the detector prototype using the same condition. The detection efficiency of the detector prototype can be calculated using the formula:

$$\eta_{SD} = \frac{N_{SD}}{N_{^3He}} \times \eta_{^3He} \tag{2}$$

Where N_{SD} is the neutron count of the detector at the special wavelength, $N_{^3He}$ is the neutron count of the ^{3}He tube at the special wavelength. The background counts need to be subtracted from

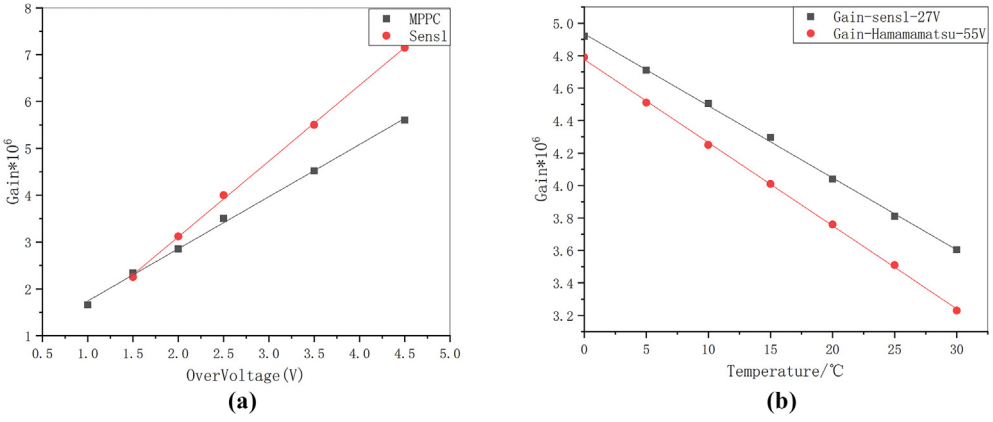

Fig. 5. (a) is the curve of gain of Hamamatsu and Sensl with over voltage at 25 °C (b) shows the temperature coefficient of SiPMs at the same over voltage.

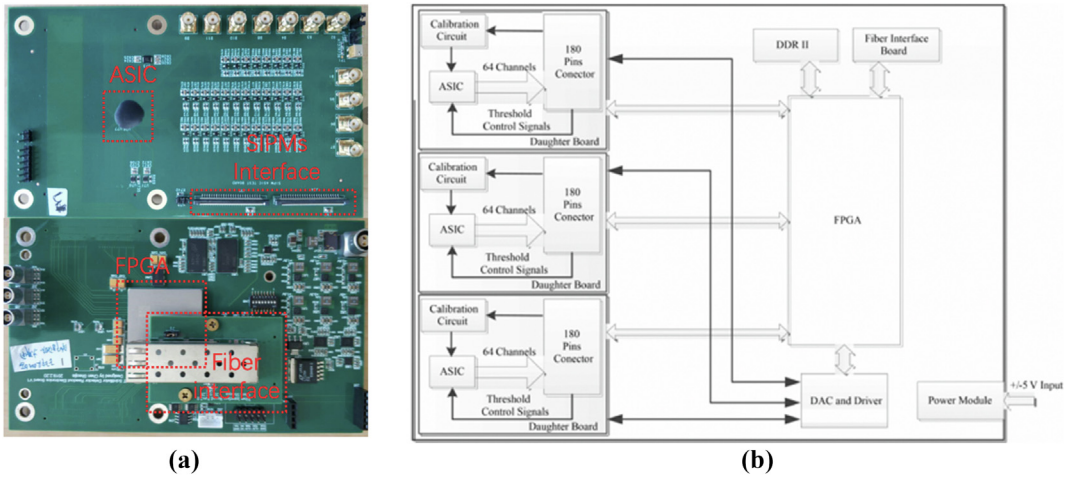

Fig. 6. (a) is a photograph of the ASIC and FPGA board. (b) shows the electronic block diagram.

both these values and they need to be normalized by the real neutron intensity obtained from the beam monitor. $\eta_{^3He}$ is the detection efficiency of the standard ^{3}He tube.

When the angle between the incident neutron and the germanium [220] monochromator is 45°, the neutrons with 1.4 Å and 2.8 Å wavelength can be obtained in the reflection angle.

Fig. 9(a) is the TOF (Time Of Flight) spectrum obtained at beam line 20. Two peaks can be obviously seen at the time of 4.9ms and 9.8ms. We can calculate the wavelength of neutrons which reflect the energy by the formula below:

$$\lambda(\mathrm{A}) = \frac{h}{\sqrt{2m_n E_n}} = \frac{h}{m_n} \times \frac{t}{L} \approx 3.9558 \frac{t(\mu s)}{L(mm)} \tag{3}$$

Where h is the Planck constant,m_n is the neutron mass, t is the TOF of the neutron, L is the distance from target to detector (13.6 m). The efficiency of the ^3He tube is 99.8% at 1.4 Å and nearly 100% at 2.8 Å. By formula (2) we can calculate the efficiency of the detector module is 80% at 2.8 Å and 64% at 1.4 Å.

The position resolution of the detector prototype is measured at the same time with this 1 mm width slit. Fig. 9(b) shows the test result with the pixel size of 3mm × 180mm.

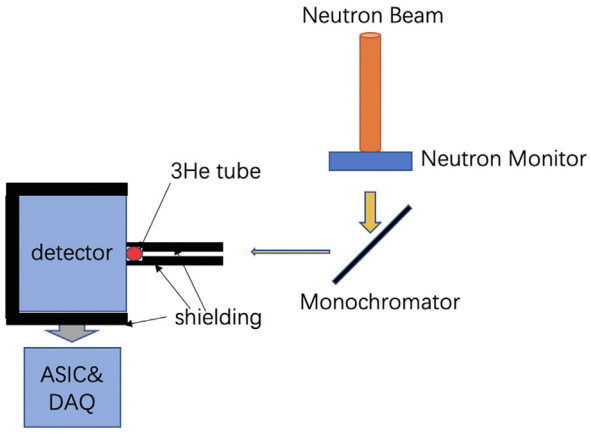

Fig. 8. The instrument layout of the efficiency measurement.

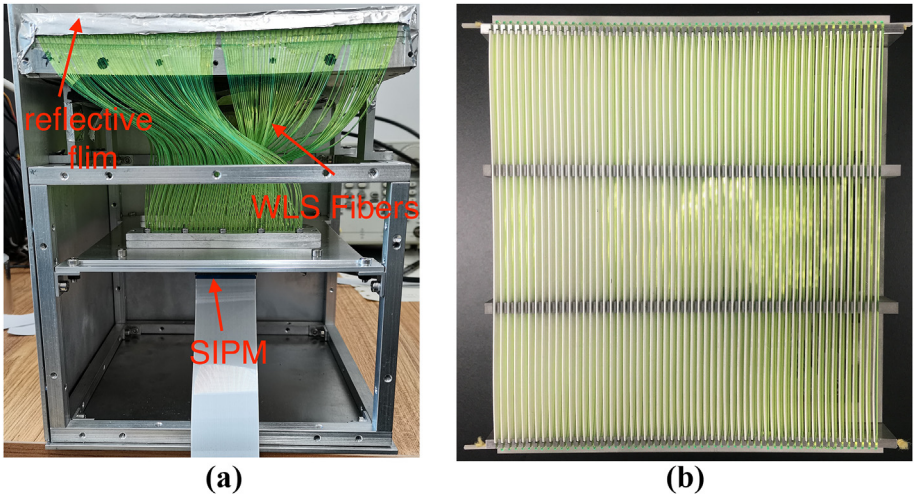

Fig. 7. 64-channel detection module (a) shows the front side of the module consisting of 64 individual singe-channel detection units, (b) is the top view of the unit which shows the 64 × 3 mm pixels without reflective films.

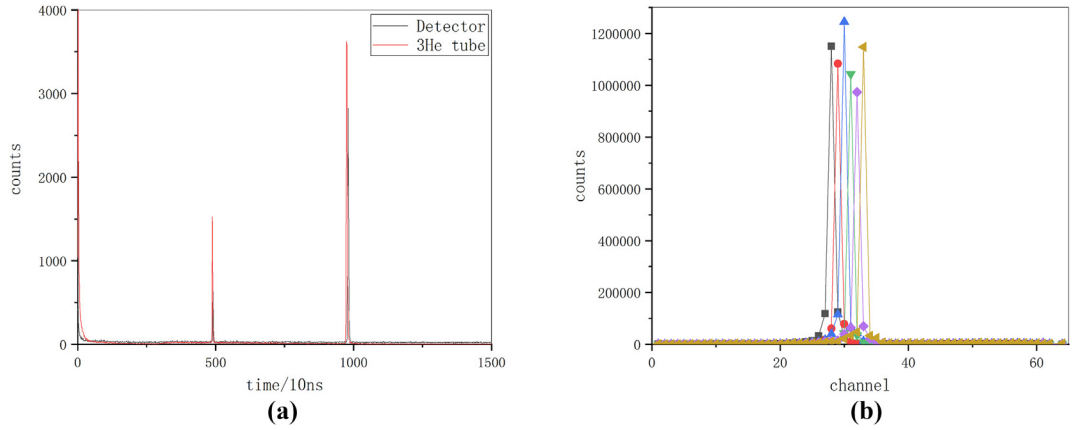

Fig. 9. (a) shows the TOF spectrum of the prototype detector and (b) is the result of position resolution scanned by the 1 mm width slits across the detector.

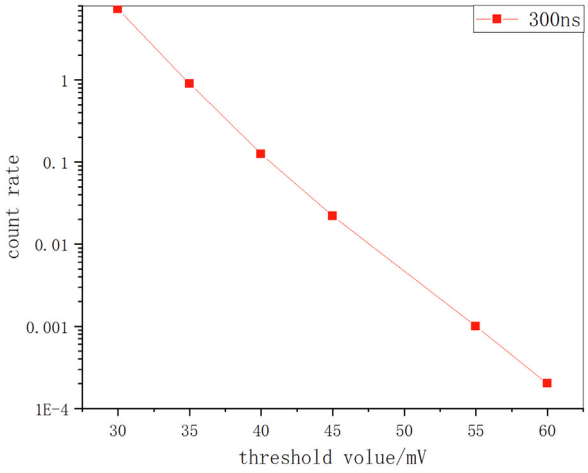

Fig. 10. The dark count rate in different thresholds.

Fig. 10 illustrates the curve of dark count rate and threshold. When the threshold value is set to 45mV and a width boundary of 300ns, the count rate can be 0.022Hz/pixel.

5. Conclusion

The SiPMs readout scintillator neutron detector has been designed for EMD. We developed a 64-ch detector prototype based on a ^{6}LiF/ZnS(Ag) scintillator, WLS fibers and SiPMs as well as its dedicated digital signal processing system based on ASIC and FPGA electronics. The characteristics of the SiPMs are measured to support the design of the neutron detector system. The detector prototype achieves the performance that the detector efficiency is larger than 40% for 1 Å, its dark count rate is 0.022Hz/pixel and the position resolution is 3mm × 180 mm. The count rate of the detector can be calculated through the TOF of detector at different neutron flux. We measured the maximum of the detector on the beam line and the value was found to be > 200kHz/pixel although the extent to which the multicounting has yet to be determined.

Since the bending radius of the WLSFs is 3mm the active area of the prototype is more than 90% compared with its structural area. This detector prototype could be a good working unit for the array splicing structure for the EMD.

Declaration of competing interest

The authors declare that they have no known competing financial interests or personal relationships that could have appeared to influence the work reported in this paper.

Acknowledgements

This worked was supported by the National Natural Science Foundation of China (No.11875273, U1832111), the Science Foundation of Guangdong (No. 2020B1515120025), the Neutron Physics Laboratory Funding of China Academy of Engineering Physics (Grant No. 2018BCE03), and the State Key Laboratory of particle Detection and Electronics Foundation.

References

[1] J. Wei, H. Chen, Y. Chen, Y. Chen, Y. Chi, C. Deng, H. Dong, L. Dong, S. Fang, J. Feng, S. Fu, L. He, W. He, Y. Heng, K. Huang, X. Jia, W. Kang, X. Kong, J. Li, T. Liang, G. Lin, Z. Liu, H. Ouyang, Q. Qin, H. Qu, C. Shi, H. Sun, J. Tang, J. Tao, C. Wang, F. Wang, D. Wang, Q. Wang, S. Wang, T. Wei, J. Xi, T. Xu, Z. Xu, W. Yin, X. Yin, J. Zhang, Z. Zhang, Z. Zhang, M. Zhou, T. Zhu, China spallation neutron source: design, R&D, and outlook, Nucl. Instrum. Methods Phys. Res. Sect. A Accel. Spectrom. Detect. Assoc. Equip. 600 (2009) 10–13, https://doi.org/10.1016/j.nima.2008.11.017.

[2] J.A. Dann, M.R. Daymond, L. Edwards, J.A. James, J.R. Santisteban, A comparison between Engin and Engin-X, a new diffractometer optimized for stress measurement, in: Physica B: Condensed Matter, Elsevier, 2004, https://doi.org/10.1016/j.physb.2004.03.139.

[3] B. Tang, Q. Yu, C. Huang, H. yun Teng, Y. feng Wang, H. Xu, Y. tao Liu, L. Qiu, G. you Wei, Z. jia Sun, The research of laser-based rapid measurement system for scintillator neutron detectors arrays, Radiation Detection Technology and Methods 4 (2020) 400–406, https://doi.org/10.1007/s41605-020-00206-9.

[4] K. Sakasai, T. Nakamura, M. Katagiri, K. Soyama, A. Birumachi, S. Satoh, N. Rhodes, E. Schooneveld, Development of neutron detector for engineering materials diffractometer at J-PARC, Nucl. Instrum. Methods Phys. Res. Sect. A Accel. Spectrom. Detect. Assoc. Equip. 600 (2009) 157–160, https://doi.org/10.1016/j.nima.2008.11.023.

[5] J.B. Mosset, A. Stoykov, U. Greuter, A. Gromov, M. Hildebrandt, T. Panzner, N. Schlumpf, A 16-ch module for thermal neutron detection using ZnS:6LiF scintillator with embedded WLS fibers coupled to SiPMs and its dedicated readout electronics, Nucl. Instrum. Methods Phys. Res. Sect. A Accel. Spectrom. Detect. Assoc. Equip. 845 (2017) 494–498, https://doi.org/10.1016/j.nima.2016.05.002.

[6] bin tang, Z. Sun, H.U.A.N.G. chang, yun Liu, H. Xu, S. Chen, X. Wang, Q. Yu, H. Teng, Y. Wang, G. Yang, Y. Chen, The neutron scintillator detector arrays (NSDA) for the GPPD in the CSNS, in: SPIE-Intl Soc Optical Eng, 2019, p. 101, https://doi.org/10.1117/12.2524697.

[7] B. Tang, Z.J. Sun, Q. Zhang, Z. Yang, H. Xu, G.A. Yang, Y.F. Wang, C. Wu, Y.B. Chen, L. Yang, Study of a position-sensitive scintillator neutron detector, Chin. Phys. C 36 (2012) 1089–1094, https://doi.org/10.1088/1674-1137/36/11/009.

[8] Instruments of CSNS in the First Target for the Neutron Scattering Experiments, IHEP, http://english.ihep.cas.cn/csns/chnl/99/index.html. (Accessed 30 August 2021). accessed.

[9] T. Nakamura, K. Toh, T. Kawasaki, K. Honda, H. Suzuki, M. Ebine, A. Birumachi, K. Sakasai, K. Soyama, M. Katagiri, A scintillator-based detector with sub-100-μm spatial resolution comprising a fibre-optic taper with wavelength-shifting fibre readout for time-of-flight neutron imaging, Nucl. Instrum. Methods Phys. Res. Sect. A Accel. Spectrom. Detect. Assoc. Equip. 737 (2014) 176–183, https://doi.org/10.1016/j.nima.2013.11.034.

[10] N. Kubota, M. Katagiri, K. Kamijo, H. Nanto, Evaluation of ZnS-family phosphors for neutron detectors using photon counting method, in: Nuclear Instruments and Methods in Physics Research, Section A: Accelerators,, Spectrometers, Detectors and Associated Equipment, 2004, pp. 321–324, https://doi.org/10.1016/j.nima.2004.05.004.

[11] J.B. Mosset, A. Stoykov, U. Greuter, M. Hildebrandt, N. Schlumpf, Digital signal processing for a thermal neutron detector using ZnS(Ag):6LiF scintillating layers read out with WLS fibers and SiPMs, Nucl. Instrum. Methods Phys. Res. Sect. A Accel. Spectrom. Detect. Assoc. Equip. 824 (2016) 319–321, https://doi.org/10.1016/j.nima.2015.11.062.

[12] A. Stoykov, J.B. Mosset, U. Greuter, M. Hildebrandt, N. Schlumpf, A SiPM-based ZnS:6LiF scintillation neutron detector, Nucl. Instrum. Methods Phys. Res. Sect. A Accel. Spectrom. Detect. Assoc. Equip. 787 (2015) 361–366, https://doi.org/10.1016/j.nima.2015.01.076.

[13] Hamamatsu Photonics. http://www.hamamatsu.com.cn/UserFiles/upload/file/20190728/2.pdf. (Accessed 30 August 2021) accessed.

[14] Sensl Photonics. https://www.onsemi.com/pdf/datasheet/microc-series-d.pdf. (Accessed 30 August 2021) accessed.

[15] R. Klanner, Characterisation of SiPMs, Nucl. Instrum. Methods Phys. Res. Sect. A Accel. Spectrom. Detect. Assoc. Equip. 926 (2019) 36–56, https://doi.org/10.1016/j.nima.2018.11.083.

[16] F. Acerbi, S. Gundacker, Understanding and simulating SiPMs, Nucl. Instrum. Methods Phys. Res. Sect. A Accel. Spectrom. Detect. Assoc. Equip. 926 (2019) 16–35, https://doi.org/10.1016/j.nima.2018.11.118.

[17] P. Achenbach, M. Biroth, W. Lauth, A. Thomas, Gain stabilization and noise minimization for SiPMs at cryogenic temperatures, Nucl. Instrum. Methods Phys. Res. Sect. A Accel. Spectrom. Detect. Assoc. Equip. 912 (2018) 110–111, https://doi.org/10.1016/j.nima.2017.10.080.